Deep reaching fluid flow in the North East German Basin: origin and processes of groundwater salinisation

M. Tesmer · P. Möller · S. Wieland · C. Jahnke · H. Voigt · A. Pekdeger

Abstract Major element chemistry, rare-earth element distribution, and H and O isotopes are conjointly used to study the sources of salinisation and interaquifer flow of saline groundwater in the North East German Basin. Chemical analyses from hydrocarbon exploration campaigns showed evidence of the existence of two different groups of brines: halite and halite Ca–Cl brines. Residual brines and leachates are identified by Br^-/Cl^- ratios. Most of the brines are dissolution brines of Permian evaporites. New analyses show that the pattern of rare-earth elements and yttrium (REY) are closely linked to H and O isotope distribution. Thermal brines from deep wells and artesian wells indicate isotopically evaporated brines, which chemically interacted with their aquifer environment. Isotopes and rare-earth element patterns prove that cross flow exists, especially in the post-Rupelian aquifer. However, even at depths exceeding 2,000 m, interaquifer flow takes place. The rare-earth element pattern and H and O isotopes identify locally ascending brines. A large-scale lateral groundwater flow has to be assumed because all pre-Rupelian aquifer systems to a depth of at least 500 m are isotopically characterised by Recent or Pleistocene recharge conditions.

Received: 28 February 2006 / Accepted: 23 February 2007
Published online: 22 March 2007

M. Tesmer · S. Wieland · A. Pekdeger
Free University Berlin,
Malteserstr. 74-100, 12249 Berlin, Germany

P. Möller
Geoforschungszentrum Potsdam 4.3,
Telegrafenberg, 14473 Potsdam, Germany

C. Jahnke · H. Voigt
Environmental Geology,
Brandenburg University of Technology Cottbus (BTU),
E. Weinert Str. 1, 03046 Cottbus, Germany

M. Tesmer (✉)
Department of Earth Science,
Institute of Geological Sciences-Geochemistry,
Hydrogeology, Mineralogy,
Malteserstr. 74-100, 12249 Berlin, Germany
e-mail: tesmer@zedat.fu-berlin.de
Tel.: +49-30-83870629
Fax: +49-30-83870740

Résumé La chimie des ions majeurs, la distribution des éléments rares et les isotopes de l'hydrogène et de l'oxygène sont utilisés conjointement pour étudier l'origine de la salinité et les flux d'eaux salées inter-aquifères dans le Bassin Nord-Est Allemand. Les analyses chimiques effectuées à l'occasion de campagnes de prospection d'hydrocarbures ont démontré l'existence de deux différents groupes de saumures : les saumures chlorurées sodiques et les saumures chlorurées sodiques et calciques. Les saumures résiduelles et les lixiviats sont identifiés par leurs rapports Br^-/Cl^-. La plupart des saumures sont issues de la dissolution des évaporites permiennes. De nouvelles analyses montrent que la répartition des éléments en traces et de l'yttrium (REY) sont étroitement liés à la distribution des isotopes de l'hydrogène et de l'oxygène. Les isotopes dans les saumures thermales issues de puits profonds et de puits artésiens indiquent des saumures évaporées, qui interagissent avec leur environnement aquifère. La répartition des isotopes et des éléments en traces prouve que des écoulements croisés existent, notamment dans l'aquifère post-rupélien. Cependant, des échanges inter-aquifères se produisent même à des profondeurs supérieures à 2000 m. La distribution des éléments en traces et les isotopes de O et H permettent d'identifier les saumures localement ascendantes. On suppose également l'existence d'un écoulement latéral à grande échelle, car les abondances isotopiques dans tous les systèmes aquifères pré-rupéliens, dont le mur est profond de 500 m au minimum, mettent en évidence des conditions de réalimentation récentes ou datant du Pléistocène.

Resumen La química de elementos mayores, la distribución de tierras raras y los isótopos de H y O han sido utilizados conjuntamente para el estudio de las fuentes de salinización y flujo entre acuíferos del agua subterránea salina en la Cuenca Noreste de Alemania. Análisis químicos de campañas de exploración de hidrocarburos mostraron evidencias de la existencia de dos grupos diferentes de salmueras: halita y halita Ca–Cl. Se han identificado salmueras residuales y lixiviados mediante la relación Br^-/Cl^-. La mayoría de las salmueras proceden de la disolución de evaporitas Pérmicas. Nuevos análisis muestran que el patrón de las tierras raras e Ytrio (REY) está directamente relacionado con la distribución isotópica de H y O. Salmueras termales procedentes de pozos

 DOI 10.1007/s10040-007-0176-y

profundos y pozos artesianos apuntan isotópicamente hacia salmueras evaporadas, que interactúan químicamente con el ambiente del acuífero. El modelo de isótopos y tierras raras prueba que existe un flujo cruzado, especialmente en el acuífero post-Rupeliano. Sin embargo, incluso a profundidades mayores de 2000 m, se produce un flujo entre acuíferos. La distribución de tierras raras y de los isótopos de H y O identifica localmente salmueras ascendentes. Se ha asumido un flujo lateral de agua subterránea a gran escala porque isotópicamente todos los sistemas acuíferos pre-Rupelianosse se caracterizan por condiciones de recarga recientes o Pleistocenas, hasta una profundidad de 500 m como mínimo.

Keywords Hydrochemistry · Rare-earth elements · Stable isotopes · Hydrostratigraphy · Brines

Introduction

The origin and compositional evolution of brines in sedimentary basins is still being debated despite decades of economic and scientific investigation. Geochemical, isotopic and hydrodynamic studies led to various theories of brine formation and movement, which were summarised by Hanor (1994a,b). The main controversy encompasses the initial sources of water and the processes by which these waters acquired their load of total dissolved solids (TDS) as high as 300–400 g/L. Carpenter (1978) suggested that the chemical composition of many deep-basin brines resembles evaporated seawater which interacted with the sedimentary rocks and/or has subsequently mixed with seawater or meteoric water. Clayton et al. (1966) published isotope data which strongly indicated that brines in several basins originated from meteoric water and not from seawater. Explanations for mechanisms allowing meteoric waters to become brines focussed on (1) salt dissolution (e.g. Bennett and Hanor 1987; Bein and Dutton 1993) and (2) shale-membrane filtration (Graf et al. 1966; Kharaka and Berry 1973).

Hydrogeological and hydrodynamic investigations also yield controversial results. The freshwater–rock-interaction model assumes that a basin's original pore water was replaced repeatedly (Toth 1980; Bassett and Bentley 1982), whereas the modified evaporation brine model implies that connate water is never displaced quantitatively (e.g. Domenico and Robbins 1985; Knauth 1988). Amalgamation of theories resulted in assumptions of coexistence and/or mixing of meteoric and modified connate waters (e.g. Knauth 1988; Senger 1991; Land and Macpherson 1992; Stueber et al. 1993). Brines are chemically altered by participation in processes of dolomitisation, albitisation, precipitation of $CaSO_4$, and ion exchange (Carpenter 1978; Spencer 1987; Wilson and Long 1992; Land 1987; Land and Macpherson 1992).

The North German Basin (NGB) is part of one of the world's largest evaporite containing sedimentary basins (Fig. 1). What makes this basin somewhat different from North American examples is the intensity of salt diapirism and the fact that glaciers covered the basin as a whole during the subsequent stages of the Pleistocene glaciations (Kloppmann et al. 2001). One of the best-studied areas in NGB is the environment of the exploratory salt mine of Gorleben, which is used for storage of high-level radioactive wastes (Klinge et al. 2002; Kloppmann et al. 2001). Grube et al. (2000) summarised the results of studies in the NGB made by Glander and Schirrmeister (1975); Hannemann and Schirrmeister (1998); Hoth et al. (1997); Kühn (1997); Lehmann (1974a,b); Löhnert et al. (1986); Naumann (2000); Trettin et al. (1997); and Voigt (1972, 1975, 1977). According to Grube et al. (2000), about 25% of the NGB is affected by inland salinisation, thought to be caused by migration of subsurface brines and saline waters through faults, fractures, or permeable geologic units. Concerning the deep-fluid circulation issue, the North East German Basin (NEGB) provides an excellent example (Fig. 1). In their studies, Hannemann and Schirrmeister (1998) concluded that near-surface salinisation originated mainly from the deeper pre-Tertiary aquifer systems. Numerical models of coupled fluid flow, heat and mass transport showed that upward solute migration takes place in the NEGB (Magri et al. 2005a,b).

This study focuses on the evaluation of two different, hydrochemical data sets: (1) unpublished data from oil prospecting and (2) additionally sampled data from shallow wells, encompassing major, minor, and trace element analyses and stable isotopes.

The aim of this study is to learn how deep brines behave, migrate and mix with less saline or fresh waters in the NEGB. Are some of the saline waters formation water in the strict sense? After rare-earth elements (REE) and yttrium distribution (henceforth combined as REY) was successfully applied in studying the various sources of thermo-saline groundwater in Israel (Möller et al. 2003), this concept is now combined with stable H and O isotopes in order to characterise saline aquifer systems.

Geologic and hydrogeologic settings

The North East German Basin (NEGB) comprises the eastern part of the North German Basin, which is part of Central European Basin System (CEBS). The NGB is bordered by the Tornquist Teisseyre Zone, to the south by the Elbe Line, and continues northwesterly into the North Sea and southeasterly into the Polish Basin (Fig. 1).

The topography of the NGB and its modern surface was formed as an intra-cratonic structure in response to, or in consequence of the Variscian orogeny (Schmidt Mumm and Wolfgramm 2002). The evolution of the basin is characterised by several stages of subsidence with its main phase during the Upper Triassic (Scheck and Bayer 1999). The basin started to form between latest Carboniferous and the Early Permian and was accompanied by the deposition of volcanic rocks (Rotliegend; Fig. 2). This igneous event was followed by a long-lasting (>250 Ma) subsidence (Scheck et al. 1999). A clastic sequence (Lower Permian, Rotliegend) of aeolian sandstones,

 DOI 10.1007/s10040-007-0176-y

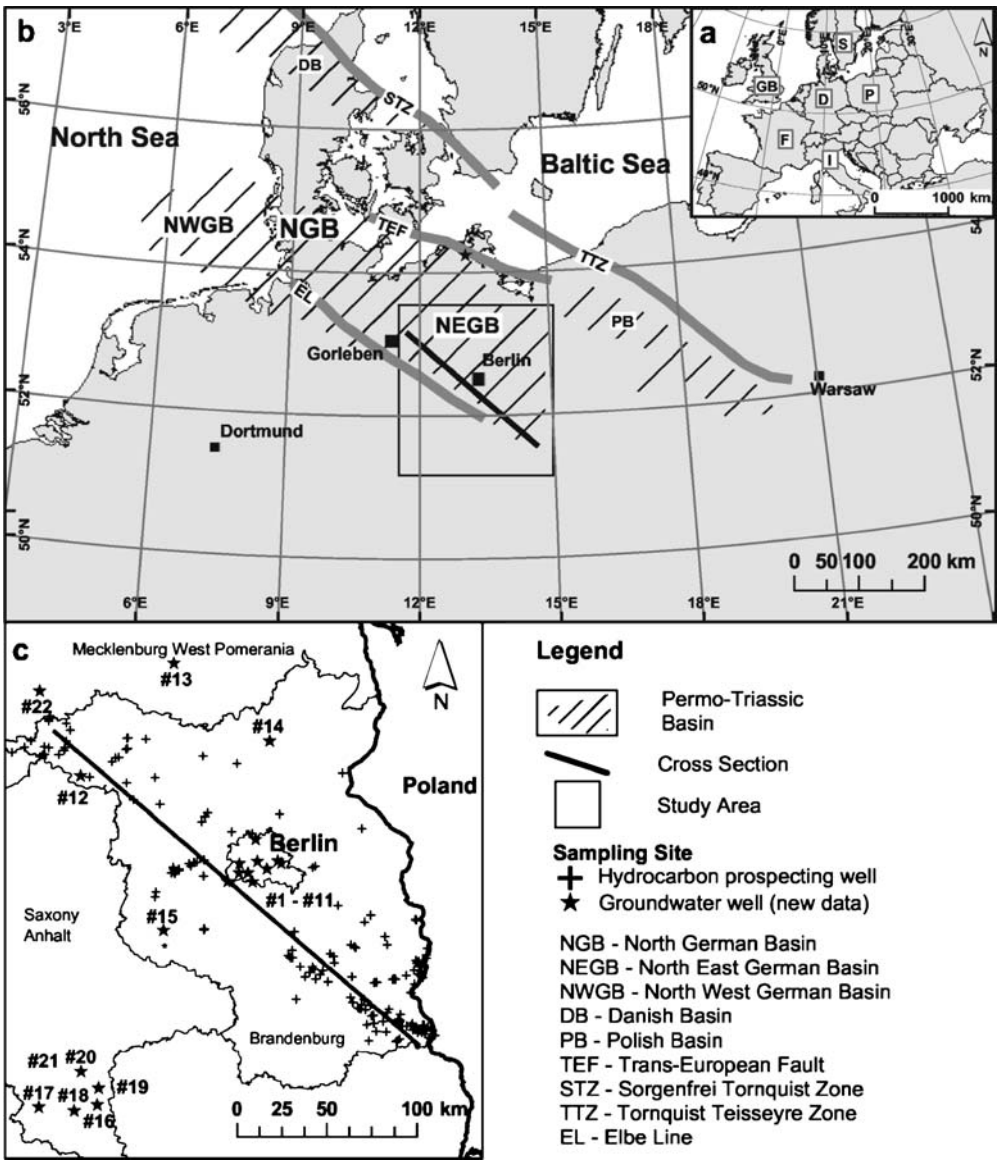

Fig. 1 **a** Map of Central Europe in which the North German Basin is located (*D* Germany, *P* Poland, *S* Sweden, etc.; The Netherlands and Denmark are not marked). **b** Sketch map of the North German Basin. **c** Groundwater sampling area. The indicated *cross-section* is given in Fig. 13

fluvial fans as well as playa deposits covered the volcanic rocks (Rieke et al. 2001). Repeated marine transgressions during Upper Permian (Zechstein) resulted in the deposition of carbonates and evaporites. In the study area, five evaporite cycles are discerned with a primary thickness of more than 1,500 m (Stackebrandt and Lippstreu 2002). In general, the thickness and composition of the beds vary widely, depending on the position in the basin. Anhydrite and halite dominate the sequences, while sylvite, carnallite and bischofite are less abundant (Kaiser 2001). Transgressions and regressions of the Tethys controlled the sedimentation in the Mesozoic, starting with terrestrial red-bed sequences (Lower Triassic: Bunter), followed by a shallow marine facies (Middle Triassic: Muschelkalk), turning into a mainly terrestrial facies of sandstones interbedded by sequences of carbonate, anhydrite, halite (Upper Triassic: Keuper) and ending in a mainly marine environment (Jurassic and Cretaceous). During the Triassic and the early Jurassic, E-W extension and the deposition of sediments initiated the movement of the underlying Zechstein evaporites (Vosteen et al. 2004). The thick Permian salt layers were mobilised and contributed to the deformation of the NGB and its differentiation into sub-basins and troughs. The intensive salt diapirism created salt pillows, walls and diapirs. Subsequent erosion complicated matters. Where salt diapirs reached the surface, they displaced the overlying sedimentary strata and generated topographic heights (Klinge et al. 1992).

The Cenozoic superficial sediments consist of unconsolidated Tertiary to Quaternary deposits, which discordantly overlay Mesozoic strata. Tertiary sediments are fluviatile sands, marine marls and clays. Quaternary deposits are highly heterogeneous due to alternating glacial and interglacial stages. Fine clayey and coarse-clastic sediments were deposited. Locally erosional channels deeply cut into the

 DOI 10.1007/s10040-007-0176-y

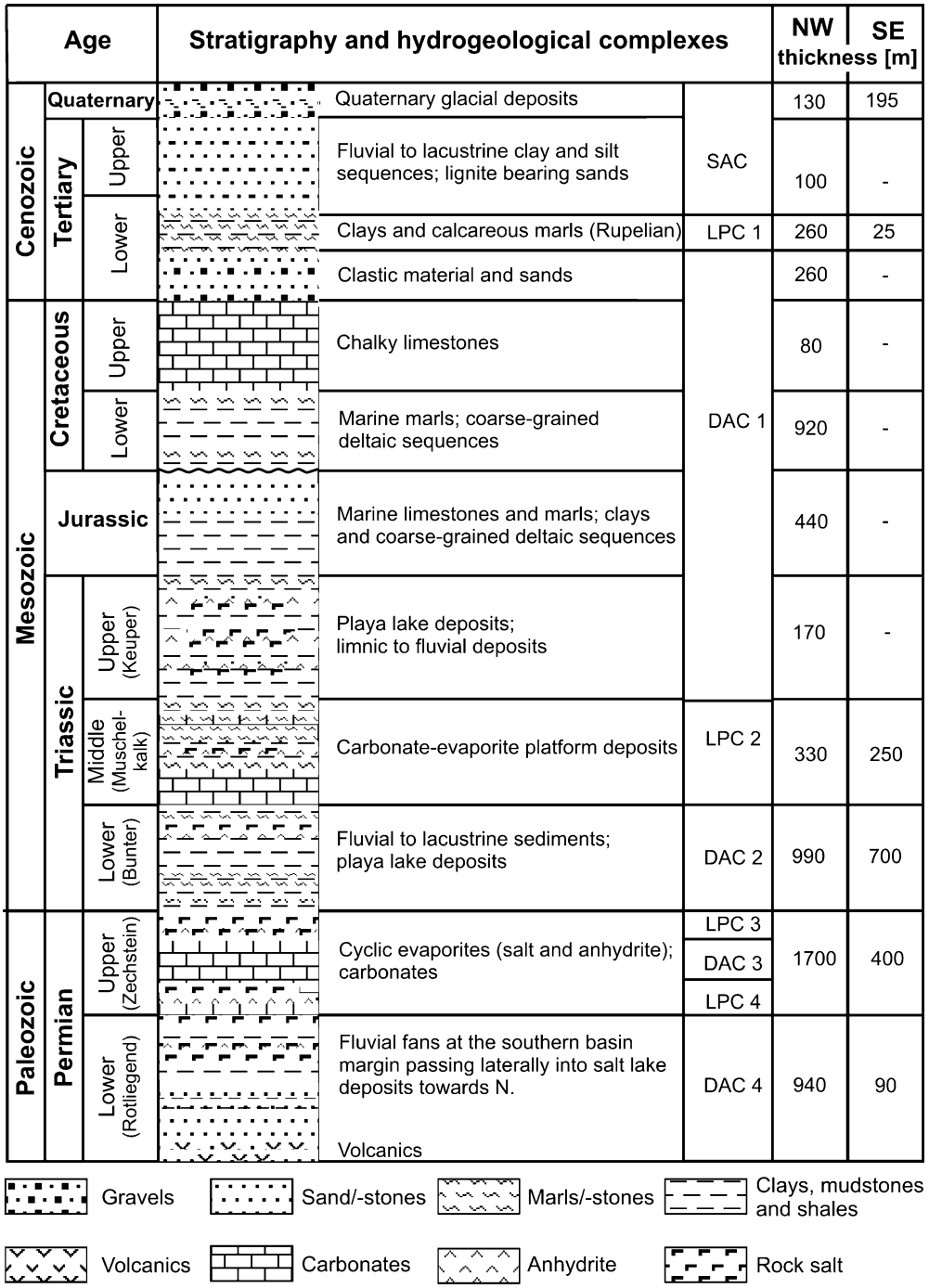

Fig. 2 Lithological and hydrogeological sequence in the North East German Basin, with *SAC* shallow aquifer complex, *LPC* low permeability complex and *DAC* deep aquifer complex; modified after Scheck and Bayer (1999)

underlying strata. As a consequence of the above processes, the occurrence, depth and thickness of most sedimentation sequences varies widely within the basin (Fig. 2).

Southward-moving glaciers moulded today's morphology during the last glaciation period (Weichsel glaciation corresponding with Wisconsin glaciation in North America). The glaciers formed the North German Plain with elevations of less than 100 m above sea level (asl). Terminal moraines stretch across the country in southeast-to-northwest direction, creating a local elevation of up to 150 m above the general level.

Summarising investigations by Manhenke (2002); Beer and Manhenke (2001); Voigt (1975) and Neumann (1975), the major aquifer complexes in the NEGB are the shallow aquifers of Cenozoic (SAC) and the deep aquifers of mainly Mesozoic to Paleozoic strata, which can be subdivided in four deeper aquifer complexes (DAC 1–4). The different aquifer complexes are separated by low-permeability complexes (LPC). The most important aquiclude with respect to groundwater management is the Rupelian Clay (LPC 1), which separates the Quaternary and Tertiary freshwater complex from the

 DOI 10.1007/s10040-007-0176-y

saline aquifer complexes below. Hydraulic connections between the freshwater body and the saline aquifer systems locally exist not only along fault zones but also along Pleistocene channels deeply cut into the underlying strata and at places where the Rupelian Clay was eroded or not deposited. The next low-permeability complex of regional importance is formed by fine-grained carbonates of Middle Triassic time, which, particularly in the central part of the basin, contain evaporatic layers of salt rock with very low permeabilities. This "impervious" unit leads to a separation of the Post-Permian strata in two aquifer systems with different hydrochemical and hydrodynamical characteristics, which are the deeper aquifer complexes of Lower Tertiary to Upper Triassic (DAC 1) and the unit of Lower Triassic (DAC 2). The Upper Permian aquifer system (DAC 3) consists of fractionated carbonate rocks which are both over- and underlain by thick confining units of salts and anhydrites (LPC 3 and LPC 4).

According to Zieschang (1974), groundwater flow in both shallow and deep aquifer systems is generally from SW to NE following the regional slope of the North German Plain towards the Baltic Sea. Discharge of brine from the deep basin aquifers and from salt dissolution zones affects the salinity of the shallow freshwater system and mainly occurs in the southern part of the investigation area, where salt meadows and saline springs are found (Hannemann and Schirrmeister 1998; Grube et al. 2000). Zieschang (1974) and Voigt (1975) favour a hydrostatically driven flow as the main force for brine movement in the NEGB. Magri et al. (2005a,b) showed by numerical simulations of transient thermohaline flow that the thermal disturbances induced by the presence of the salt diapirs also lead to an upward-directed flow of brines in the NEGB.

Hydrochemical studies of the deeper aquifer systems suggest that fluids are highly heterogeneous and multiple sources of salinity exist in the NGB (e.g. Warren and Smalley 1992; Nishri et al. 1988; Kloppmann et al. 2001; Grube and Lotz 2004). The high salinity of the deep aquifer systems is mainly explained by the infiltration of meteoric water dissolving salt bodies, connate water dissolving salt bodies during the stage of salt diapirism and the existence of Permian evaporation brines.

In summary, hydrodynamic and hydrochemical behaviour of brines are highly variable within the different aquifer complexes of the NGB. Especially the intensity of salt diapirism lead to a complex geological environment with preferential flow paths and a strong interaction between the temperature distribution, salt concentrations and groundwater flow fields. Subsequent erosion and glaciations complicated matters. Different flow regimes and the existence of different brines resulted in water–rock interaction and mixing with meteoric waters, which is similar to processes in the North American and Canadian sedimentary basin systems (Carpenter 1978; Stueber et al. 1993; Knauth 1988; Bein and Dutton 1993; Land 1992; Connolly et al. 1990; Evans and Nunn 1989; Bennett and Hanor 1987; Mehta et al. 2000).

Sampling and analytical procedure

The majority of water analyses used in this study were performed for hydrocarbon prospecting in the former German Democratic Republic in the 1970s. These analyses were taken from the data files of the Geological Survey of Berlin-Brandenburg and of commercial companies; until recently, data from these files were subject to restricted access. These analyses comprise 291 samples which cover (1) the diversity of brines, and (2) the various deep aquifers. The locations are not evenly distributed in the study area but are largely oriented along the margin of the NEGB, from its SE corner to its centre in the NW (see SE–NW cross-section in Fig. 1). Water samples with a charge balance error of more than 5% were excluded from further investigation (13 samples). Samples with a charge balance error of 0 were retained, although that indicates that one or more ions (e.g. Na^+ and K^+) were determined from the charge balance (20 samples).

This set of analyses is supplemented by new analyses of groundwaters from production and observation wells in the Federal States of Germany: Berlin, Brandenburg and Saxony Anhalt, Mecklenburg West Pomerania (stars in Fig. 1; Table 1). All wells were pumped until the physico–chemical conditions—EC, electrical conductivity), pH, T, Eh (redox potential), O_2—were constant, i.e. steady-state conditions were achieved in the majority of cases. The physico–chemical parameters were measured directly in a flow unit. Water samples for anions, cations and REE were filtered online through 0.2-µm cellulose-acetate filters (Sartobran, Sartorius, Germany). Samples for cation analysis were preserved with concentrated nitric acid (HNO_3) at pH<2. Alkalinity was determined by Gran titration immediately after sampling. Cations were measured by atomic absorption spectrometry (Perkin Elmer 5000, USA) and anions were measured using ion chromatography (DX 100). The water samples are characterised in Table 1.

For later discussion, Cl^-_{excess} has to be defined Eq. (1), which denotes the equivalents of Cl^- that are unbalanced by alkalis:

$$Cl^-_{excess} = Cl^- - Na^+ - K^+ \quad (1)$$

All concentrations have to be given in meq/L.

For preconcentration of REY and their separation from the major components, waters are adsorbed onto organophosphates on a porous matrix at pH 2 (Bau and Dulski 1996; Hennebrüder et al. 2004). This method was described by Shabani et al. (1990). When applying this preconcentration method to groundwaters with enriched Ca contents (>0.01 molar), the proposed method yields incomplete recoveries of light REE at pH 2. In such cases, the pH has to be as high as 4 (Möller et al. 2005).

Two to ten hours after pH adjustment the waters were passed through preconditioned SepPakC_{18} cartridges (Water Corp., USA) that contain an adsorbate of a mixture of different ethylhexylphosphates (Merck, Ger-

 DOI 10.1007/s10040-007-0176-y

Table 1 Sampling locations and hydrochemical classification of groundwaters in the NE German Basin

Stratigraphy	Depth (m)	TDS (g/L)	Degree of salinisation	Water type	Location and sample ID no.	Federal State of Germany
Quaternary	88	0.5	fresh	Ca–Na–HCO_3	Fabeckstr. (shallow) no. 5	Berlin
Upper Tertiary	169	5.1	brackish	Na–Cl	Fischerhütten-weg no. 8	Berlin
	203	2.4	brackish	Na–Cl–HCO_3	Fabeckstr. (deep) no. 4	
Low-permeability complex of Tertiary (Rupelian)						
Lower Tertiary	281	23	saline	Na–Cl	Osdorferstr. no. 6	Berlin
Cretaceous	222	0.8	fresh	Na–HCO_3	Köpenickerstr. no. 1	Berlin
	230	9.0	brackish	Na–Cl	Friedrichsfelde no. 2	
Jurassic	185	18	saline	Na–Cl	Lübars no. 10	Berlin
	278	28	saline	Na–Cl	Unstrutstr. no. 3	Berlin
	300	30	saline	Na–Cl	Reichstag no. 11	Berlin
	1616	163	brines	Na–Cl	Templin no. 14	Brandenburg
Upper Triassic (Keuper)	127	8.1	brackish	Na–Cl–SO_4	HMI no. 7	Berlin
	218	46	saline	Na–Cl	Postfenn no. 9	Berlin
	773	191	brines	Na–Cl	Belzig no. 15	Brandenburg
	1000	160	brines	Na–Cl	Bad Wilsnack no. 12	Brandenburg
	1500	155	brines	Na–Cl	Waren no. 13	Mecklenburg West Pomerania
	2250	219	brines	Na–Cl	Neustadt-Glewe no. 22	
Low-permeability complex of Triassic (Lower Keuper, Muschelkalk)						
Lower Triassic (Bunter)	23.2	1.4	brackish	Ca–Mg–SO_4–HCO_3	Leiha no. 18	Saxony Anhalt
	80	0.5	fresh	Ca–Mg–Na–HCO_3	Nebra no. 17	
	95.5	1.3	brackish	Na–HCO_3–SO_4	Hy AI 394 no. 20	
Low-permeability complex of Upper Permian (Zechstein)						
Upper Permian (Zechstein)	100	75	saline	Na–Cl	Amsdorf Sportplatz no. 21	Saxony Anhalt
	186.5	184	brines	Na–Cl	Most 4363 no. 19	
	251	87	saline	Na–Cl	Bad Dürrenberg no. 16	

Degree of salinisation according to Carpenter (1978)

many) acting as a liquid cation exchanger. The cartridges were enclosed in parafilm for storage and transportation. In the laboratory, the cartridges from the field loaded with REY were washed with 50 ml 0.01-M sub-boiled HCl, and the REY were eluted with 40 ml 6-M sub-boiled HCl at a rate of 3 ml/min. After evaporation to dryness, the residues were taken up by 1 ml of 5-M sub-boiled HNO_3. These solutions were spiked by a Ru-Re mixture for possible corrections of the internal shift of the response factors in inductively coupled plasma mass spectrometry (ICP-MS) measurements if necessary (Bau and Dulski 1996) and filled up to 10 ml with purified water. Dulski (2001) gives further details of the measurements. Calibration solutions were prepared from single-element standard solutions (CertiPUR ICP standards (Merck, Germany) traceable to SRM (Standard Reference Materials) from NIST (National Institute of Standards and Technology)). Several corrections were necessary because of interferences of molecular ions with the desired mono-charged ions of the REE (Dulski 1994). Blank corrections for La, Ce, and Pr, which are contaminants of the commercially available liquid cation exchanger (Merck, Germany), were necessary. In geothermal fluids, $^{139}La^{+}$ had to be corrected for $^{123}Sb^{16}O^{+}$ (Möller et al. 2003). The efficiency as determined by either Tm single spike or Pr-Tm double spike varies between 93 and 104%. Results are presented in Table 2.

The REY were measured using an ELAN 5000 Perkin Elmer ICP-MS at the GeoForschungsZentrum Potsdam, Germany. REY abundances are given in pmol/L. REY abundance is conventionally displayed as REY patterns. In these patterns, normalised REY concentrations are plotted vs. the atomic number of REY. Because of its similarity with Ho, Y is placed after Ho (Rizkalla and Choppin 1991). Y and Ho can be considered as geochemical twins (Bau 1999). In this contribution, C1 chondrite normalisation is applied because this reference material is the least fractionated with respect to REY (Anders and Grevesse 1989).

Samples for stable O and H isotopes were taken without any further treatment. The measurements of $^{18}O/^{16}O$ ratios and $^{2}H/H$ ratios were performed using a Delta-S mass spectrometer (Finigan) at the Alfred Wegner Institute (AWI) Potsdam, Germany. H isotopes were determined by a H_2 equilibration and O isotopes were equilibrated with CO_2. Meyer et al. (2000) describe the measurement routines in detail. All isotope results are reported in $\delta^{2}H$ and $\delta^{18}O$ notation, representing per mil (‰) deviation from the VSMOW (Vienna Standard Mean Ocean Water).

 DOI 10.1007/s10040-007-0176-y

Table 2 Chemical composition of groundwater samples taken at observation and production wells in the German federal states of Berlin, Brandenburg, Saxony-Anhalt, Mecklenburg-West Pommerania (MWP)

	Berlin											Brandenburg				Saxony-Anhalt					MWP	
Locatity	Köpenickerstr.	Alt Friedrichs-felde	Unstrutstr	Fabeckstr. (deep)	Fabeckstr. (shallow)	Osdorferstr.	HMI	Fischerhütten-weg	Postfenn	Lübars	Reichstag	Bad Wilsnack	Waren	Templin	Belzig	Bad Dürren-berg	Nebra	Leiha	Most 4363	Hy AI 394	Amsdorf Sportplatz	Neustadt Glewe
Sample ID no.	1	2	3	4	5	6	7	8	9	10	11	12	13	14	15	16	17	18	19	20	21	22
pH	7.95	7.97	7.2	7.05	7.06	7.04	7.65	7.77	7.26	7.67	6.91	6.05	5.64	7.55	6.1	6.51	7.56	6.91	6.39	9.47	7.14	5.11
T	12.9	16.5	15.2	11.5	11.0	11.2	15.1	10.1	15.9	15.2	59.3	19.3	58.0	1.08	21.7	16.5	10.1	10.8	14.5	8	10.6	77.4
Na^+	6.9	144	418	34.4	2.2	370	109	73.08	639	270	452	2488	2388	2545	3088	1309	1.7	3.2	3045	16.4	1035	3084
K^+	0.19	0.48	1.14	0.16	0.06	1.02	0.52	0.28	1.74	0.92	1.33	8.18	4.86	7.42	9.59	8.29	0.16	0.20	19.2	0.23	8.44	19.4
Mg^{2+}	1.15	4.11	18.1	0.64	0.66	9.87	5.76	2.14	29.6	10.5	20.6	86.4	70.8	90.5	90.5	31.3	1.81	7.40	65.0	0.04	59.6	119
Ca^{2+}	2.0	3.09	17.5	1.05	3.19	7.98	9.98	3.99	62.9	7.98	15.0	120	135	110	69.9	96.3	2.84	9.48	104.8	0.07	130	449
Cl^-	1.78	144	449	28.9	0.20	382	87.4	73.6	691	299	508	2759	2691	2768	3196	1382	0.23	3.47	2962	1.35	1241	3824
SO_4^{2-}	0.06	0.40	27.1	1.46	0.06	11.4	41.6	3.64	93.7	4.16	6.41	25.0	23.9	56.2	79.94	101	0.40	9.58	115	4.58	61.2	18.7
HCO_3^-	8.25	8.10	4.50	7.85	5.90	8.91	3.23	8.30	7.70	6.30	4.60	2.70	2.10	2.90	4.35	5.00	5.75	7.90	3.13	11.1	0.10	2.25
Br^-	0.01	0.04	0.15			0.10	0.03	0.03	0.69	0.14	0.24	1.53	1.46	1.61	0.81	0.25			0.72		0.36	1.66
La	9.49	1.35	61.6	2011	26.9	10.6	48.5	16.1	171	18.6					55.30	21.6	20.2	3.29	232	10.6		
Ce	25.6	2.66	97.9	4028	65.3	18.4	74.1	46.1	502	34.6	5.75	176	118	252	209.8	43.7	55.5	12.9	652	28.0	10.0	
Pr	2.71	0.32	9.87	433	7.12	2.00	7.22	5.29	53.9	3.72	0.75	26.1	28.5	35.1	18.47	4.94	4.99	1.45	48.2	3.50		
Nd	11.2	0.96	42.0	1830	30.7	8.27	27.8	22.3	229	15.9	3.28	132	207	170	76.6	21.9	23.0	6.34	203	14.9	10.6	
Sm	2.33		7.64	366	6.42	1.68	4.62	5.70	48.7	3.59	0.79	33.2	61.2	36.6	15.22	5.21	5.18	1.35	33.1	3.93	4.13	
Eu	0.57		2.04	92.4	1.30	0.48	1.33	1.40	12.8	0.88	0.23	9.42	16.6	9.41	4.38	1.51	1.54	0.40	8.78	1.20	1.20	
Gd	2.51	0.40	11.0	415	7.17	2.75	6.71	6.33	61.2	4.71	1.09	55.2	72.0	51.9	26.1	7.84	7.85	1.93	52.1	5.40	5.00	629
Tb	0.37	0.07	1.70	59.4	1.00	0.42	0.87	1.05	10.0	0.83	0.16	6.96	6.26	5.85	3.89	1.27	1.54	0.31	6.54	0.95	0.56	63.4
Dy	2.31	0.64	13.4	360	7.73	3.78	6.65	7.77	67.2	6.99	1.13	33.7	25.1	29.7	25.6	8.43	12.6	2.40	42.0	7.43	3.13	228
Y	32.6	14.2	316	4824	139	82.6	139	119	884	157	21.2	492	358	430	485	167	273	49	1202	215	69.3	3080
Ho	0.48	0.15	3.58	75.5	1.81	1.02	1.67	1.74	14.8	1.78	0.27	6.06	3.66	5.40	5.80	1.93	3.38	0.63	10.6	1.96	0.66	30.8
Er	1.36	0.55	12.56	226	6.15	3.65	5.30	6.25	47.36	6.01	0.75	13.8	7.42	12.6	16.1	5.41	11.3	2.28	31.7	6.39		56.6
Yb	1.08	0.44	11.2	179	6.69	3.89	4.69	6.43	47.3	5.66	0.61	6.95	3.22	7.55	11.5	3.79	10.5	2.20	24.6	6.17	1.21	23.3
Lu	0.15	0.07	1.87	29.1	1.17	0.66	0.77	1.09	7.78	0.88	0.09	1.03	0.47	1.08	1.76	0.59	1.61	0.36	4.16	1.07	0.21	3.23
$\delta^{18}O$	−8.73	−9.43	−9.04	−9.34	−9.04	−8.95	−10.60	−9.85	−7.35	−8.54	−8.28	−3.62	−3.45	−3.97	−7.67	−9.58	−9.72	−9.24	−9.80	−11.13	−8.84	−1.72
$\delta^{18}O_{corrected}$	−8.73	−9.42	−9.04	−9.34	−9.04	−8.95	−10.61	−9.86	−7.35	−8.54	−8.27	−3.60	−3.42	−4.15	−7.66	−9.57	−9.72	−9.24	−9.81	−11.13	−8.83	−1.67
δ^2H	−61.56	−66.35	−60.76	−67.86	−64.06	−61.89	−76.13	−72.26	−50.98	−58.00	−54.64	−26.36	−27.28	−24.30	−49.74	−66.89	−68.09	−66.69	−66.64	−81.07	−63.17	−26.6
$\delta^2H_{corrected}$	−61.62	−66.33	−60.65	−67.88	−64.10	−61.87	−76.18	−72.26	−50.87	−57.94	−54.52	−25.79	−26.66	−30.11	−49.55	−66.74	−68.09	−66.69	−66.88	−81.10	−62.72	−24.95
R-type	2	1	1	2	1	1	2	2	2	1	2	3	3	3	2	2	1	1	2	1	3	3

Y yttrium. The rare-earth elements (REE) include La, Ce, Pr, Nd, Sm, Eu, Gd, Tb, Dy, Ho, Er, Yb, Lu. The major ions concentrations are given in meq/L, REY in pmol/L and isotopes in (‰) deviation from Vienna Standard Mean Ocean Water (VSMOW). No values are given when either not measured or classified, or in the case of REY, the necessary corrections exceeded 30% of the initial intensities of REY in ICP-MS measurements.

DOI 10.1007/s10040-007-0176-y

The reproducibility of δ^2H and $\delta^{18}O$ are ±0.8 and ±0.1‰, respectively. The determinations of δ^2H and $\delta^{18}O$ in highly mineralised waters were corrected by the empirical formula, Eqs. (2 and 3), following the investigation of Bourg et al. (2001) for monovalent salts (here NaCl):

$$\delta^2H_{corrected} = \delta^2H_{meassured} - 2.285 \times Na^+ \quad (2)$$

$$\delta^{18}O_{corrected} = \delta^{18}O_{meassured} - 0.0724 \times Na^+ \quad (3)$$

Na^+ concentrations have to be given in mol/L.

The studies showed that the so-called isotope salt effect varies linearly with the molality of the solution for δ^2H and $\delta^{18}O$. The given relations were determined for molarities between 0.029 and 2.9.

Results

Major components

The variation of total dissolved solids (TDS) in the NEGB is displayed in Fig. 3. Taking into account the stratigraphic sources of samples, any depth relationship is absent. Two groups are distinguishable. Group 1 comprises samples from the DAC 1 (Lower Tertiary to Upper Triassic) strata but also includes a few samples from other strata. TDS increases to 270 g/L at depths of 2,300 m and shows significant correlation with depth. For the majority of samples, the gradient steepens at a depth of about 800 m.

Group 2 assembles brines from Upper and Lower Permian (DAC 3 and DAC 4) and Lower Triassic (DAC 2) strata without any correlation between depth and TDS. Ranging from 250 to 350 g/L, the mineralisation of these waters is by far higher than in group 1.

Groundwaters from DAC 3 are present in both groups. They display steep gradients of TDS above 1,000 m but none below (Fig. 3). The samples from DAC 3 and DAC 4 are rather uniform in TDS. From Fig. 3, it is evident that stratigraphic units are not related to depth. Depending on the position of wells in the basin, margin or centre, depth of occurrence and thickness of geological formations vary widely. For example, Permian aquifers are present at any depth because of salt diapirism.

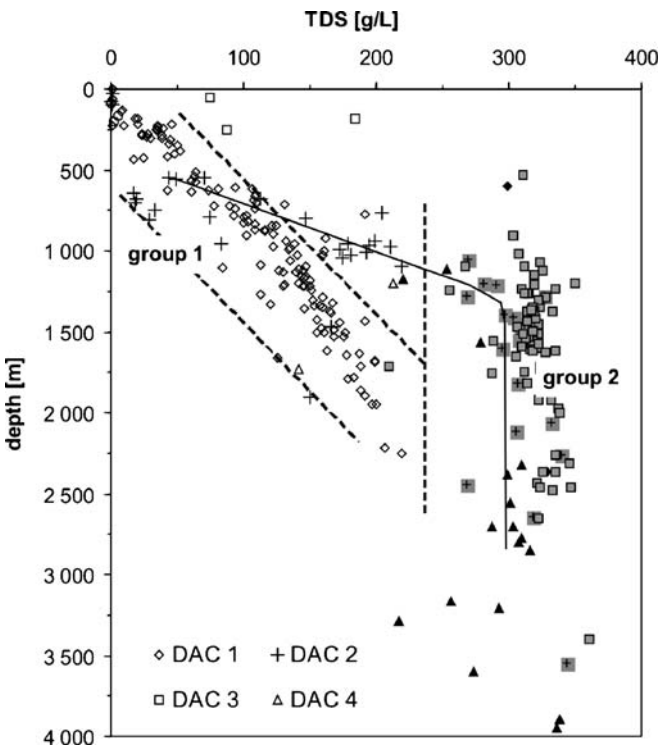

Fig. 3 Cross-plots of total dissolved solids (TDS) in g/L vs. sampling depth in m; the *symbols* indicate both the associated deep aquifer complex (*DAC 1–4* in Fig. 2) and the grouping for samples of group 1 (*open symbol*) and for samples of group 2 (*shaded symbol*). The *solid line* delineates the depth salinity trend in samples of Lower Triassic (*DAC 2*)

Element cross-plots prove the existence of two groups of saline waters (Fig. 4). In all samples, HCO_3^- content is negligibly low (<15 meq/L) and SO_4^{2-} concentration rarely exceeds 150 meq/L. In group 1, Na^+, Br^-, Ca^{2+}, and Mg^{2+} show a strong correlation with Cl^-, whereas data scatter widely in group 2. Group 1 is dominated by Na^+ and Cl^- with values up to 3,300 and 3,700 meq/L, respectively. Ca^{2+} concentrations range from 50 to 150 meq/L, whereas Mg^{2+} concentrations vary between 10 and 180 meq/L.

In group 2, Na^+ may reach 5,000 meq/L but is no longer the dominant cation. Mg^{2+} and Ca^{2+} concentrations vary between 24 to 9,700 meq/L and 26 to 3,400 meq/L, respectively. In this group, because Mg^{2+} dominates the cation composition with more than 90%, two samples stand out.

The majority of samples do not plot along the seawater evaporation line after Fontes and Matray (1993). In the cross plots of SO_4^{2-} vs. Cl^- both groups cover wide arrays without overlap. This is different in the cross plots of Ca^{2+} vs. SO_4^{2-} and Mg^{2+}, where the arrays overlap considerably (Fig. 5). Most data show Ca^{2+}/SO_4^{2-} equivalent ratios <1 (Fig. 5a) independent of their reservoir. Besides samples from DAC 3, all samples have Ca^{2+}/Mg^{2+}-equivalent ratios close to unity or >1.

In cross-plots of $\left(Ca^{2+} + Mg^{2+}\right)/Cl^-_{excess}$ vs. Cl^-_{excess} all samples with high Cl^-_{excess} plot along the line representing $\left(Ca^{2+} + Mg^{2+}\right)/Cl^-_{excess}$ equivalent ratios of 1 signalling the presences of (Ca, Mg)Cl_2 (Fig. 6). These brines are highly variable in Ca^{2+}/Mg^{2+} equivalent ratios ranging from <1 to >100 (Fig. 5b). Any ratio significantly above and below unity indicates the presence of earth alkaline bicarbonate and sulphate and alkaline carbonates and sulphate, respectively. Comparing Fig. 6a and b, it turns out that at low Cl^-_{excess} values, alkali carbonates and sulphate water are present in group 1, whereas earth alkaline carbonates and sulphates occur in group 2. Note the different scales in Fig. 6.

 DOI 10.1007/s10040-007-0176-y

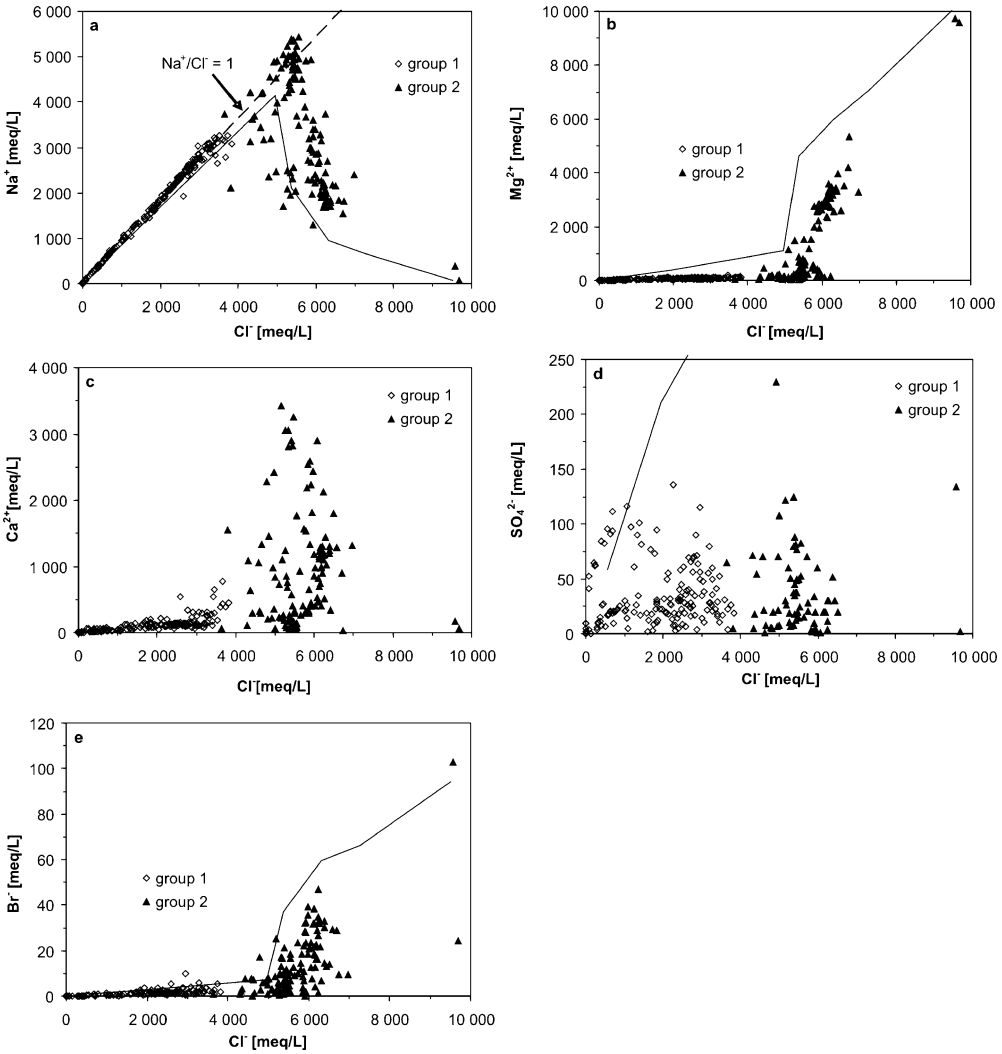

Fig. 4 Cross-plots of **a** Na^+, **b** Mg^{2+}, **c** Ca^{2+}, **d** SO_4^{2-} and **e** Br^- vs. Cl^- in meq/L. Grouping is according to Fig. 3. The *curve* represents the seawater evaporation trend based on the literature compilation in Fontes and Matray (1993)

In Fig. 7, the earth alkaline to alkali equivalent ratio $(Ca^{2+}+ Mg^{2+})/(Na^+ + K^+)$ is plotted vs. Cl^-_{excess}. Both groups show a strong correlation between the chosen parameters. The vertical spread of samples of group 1 (Fig. 7a) is caused by dissolution of either Ca-carbonates and sulphate or decreasing dissolution of halite which both leads to Ca^{2+}/Mg^{2+} equivalent ratio of >1 (Fig. 5a). Only the very low-salinity samples are Ca-bicarbonate and -sulphate waters. In Fig. 7b, an increasing positive trend is displayed with only the DAC 4 samples following a slightly different trend. The equivalent ratios exceed by far those of group 1. Note the different scale.

The Br^-/Cl^- equivalent ratios of water samples show different arrays for groups 1 and 2, although they both start with about the same values, near the Na^+/Cl^- equivalent ratio of 1 (Fig. 8). For orientation, the seawater evaporation line is given. The majority of samples of group 1 display Br^-/Cl^- below the seawater ratio of 1.5. Both groups start with dissolution of halite. Group 1 is terminated when reaching the seawaters ratio of Br^-/Cl^-, whereas group 2 develops to higher Br^-/Cl^- and lower Na^+/Cl^- ratios, but almost all samples plot below the seawater evaporation line (Fontes and Matray 1993). The spread in Na^+/Cl^- and Br^-/Cl^- equivalent ratios in group 2 is significantly larger than in group 1. The distribution of samples in group 2 show distinct distribution with reference to their aquifers of origin.

Rare-earth elements and yttrium (REY)

The normalised REY patterns show smooth trends in which Ce, Eu, Gd and Y behaves anomalously. Grouping REY patterns according to their trends, at least three general types are discernable (Fig. 9):

1. Type R1. Patterns decrease from La to Eu and increase from Eu to Lu (denoted concave patterns). This type comprises groundwaters from Quaternary, Tertiary, Jurassic, Upper Triassic (Keuper), and Lower Triassic (Tables 1 and 2).
2. Type R2. REY patterns decrease from La to Eu, and flatten thereafter towards Lu. This type comprises waters from Cretaceous to Upper Permian aquifers (Tables 1 and 2).

 DOI 10.1007/s10040-007-0176-y

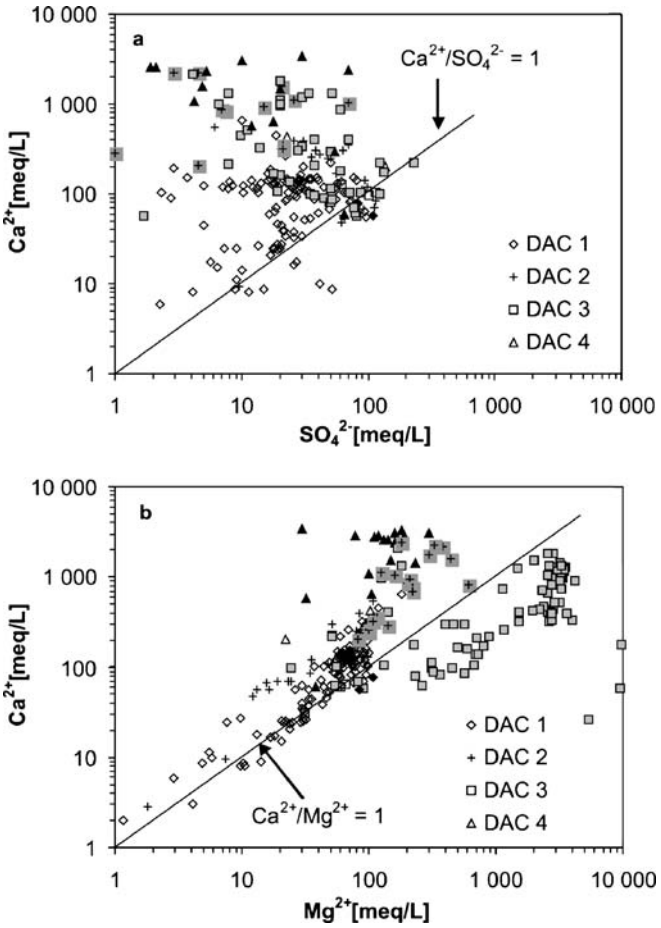

Fig. 5 Cross-plots of **a** Ca^{2+} vs. SO_4^{2-} and **b** Ca^{2+} vs. Mg^{2+} in meq/L. *Symbols* are according to Fig. 3

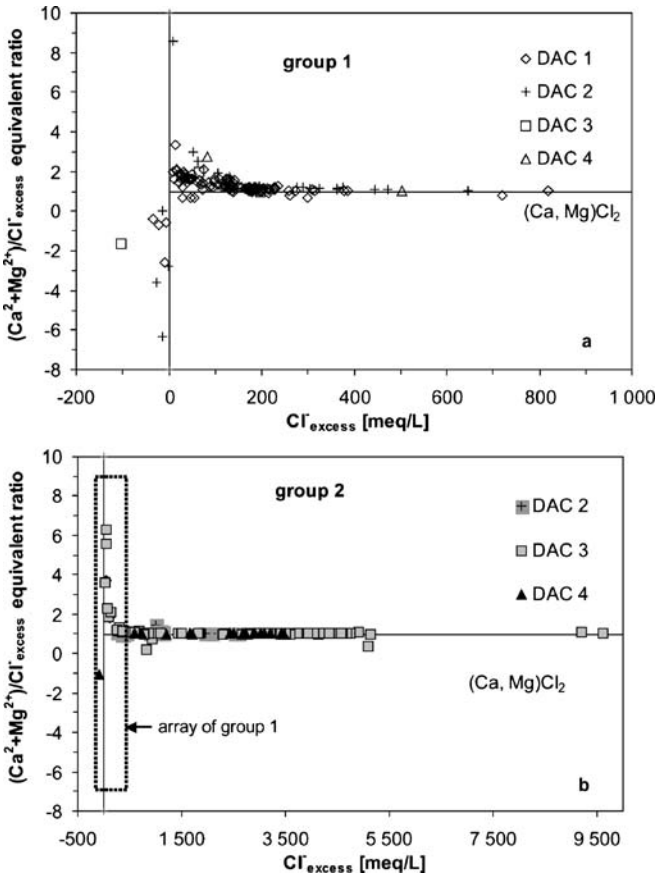

Fig. 6 Cross-plots of $(Ca^{2+} + Mg^{2+})/Cl^-_{excess}$ equivalent ratio vs. Cl^-_{excess} in meq/L in the deep aquifer complexes (DAC 1–4 in Fig. 2) for samples of **a** group 1, and **b** group 2. Symbols are according to Fig. 3

3. Type R3. This type comprises patterns with decreasing trends from Eu to Lu. These waters stem from Jurassic to Upper Permian aquifers. The incomplete REY pattern of no. 22 shows exactly the same trend as the others but at enhanced level.

Stable isotopes

In environments with regular recharge of groundwater throughout the year, the isotopic composition of groundwater closely reflects the weighted average annual precipitation. With its flat morphology in NEGB (absence of altitude effects), δ^2H and $\delta^{18}O$ values depend largely on local climatic conditions. The average isotope composition of modern groundwater in the NGB is −8.00‰ for $\delta^{18}O$ and −60.0‰ for δ^2H, values which resemble the present-day average of the annual isotope composition of precipitation in Berlin (δ^2H: −55.0‰; $\delta^{18}O$: −7.70‰).

In the cross-plots of δ^2H vs. $\delta^{18}O$, most of the samples plot near to the global meteoric water line (GMWL; Craig 1961; Fig. 10). For comparison, the results of Kloppmann et al. (2001) for saline waters around the Gorleben diapir (Fig. 1) are indicated by an array. Most of the data lie in the typical range of regional meteoric waters. The highest isotope ratios ($\delta^2H > -30$‰, $\delta^{18}O > -5$‰) characterise brines from Jurassic to Upper Triassic strata and plot right to the GMWL. The brackish waters show the lowest values ($\delta^2H < -70.0$‰, $\delta^{18}O < -10.00$‰) (Tables 1 and 2), which characterises mixing with Pleistocene recharge (Trettin et al. 1997; Kloppmann et al. 2001).

Discussion

Major elements

In Fig. 4a the vertex of the evaporation curve indicates the beginning of halite precipitation, which leads to depletion of Na^+, whereas most other ions are further enriched by evaporation. Any water encountered beyond this point is a highly concentrated brine. Data of group 1 do not plot along the evaporation line but follow more closely the halite dissolution line. None of the waters of group 1 reaches the stage of halite saturation. Contrastingly, most of group 2 waters plot beyond the stage of halite saturation. Higher Na^+ values than those of the evaporation curve are caused by enhanced solubility of halite at enhanced temperatures of these deep waters.

The variability of Ca^{2+}/Mg^{2+} equivalent ratios (Fig. 5b) and the constancy of $(Ca^{2+} + Mg^{2+})/Cl^-_{excess}$ (Fig. 6)

 DOI 10.1007/s10040-007-0176-y

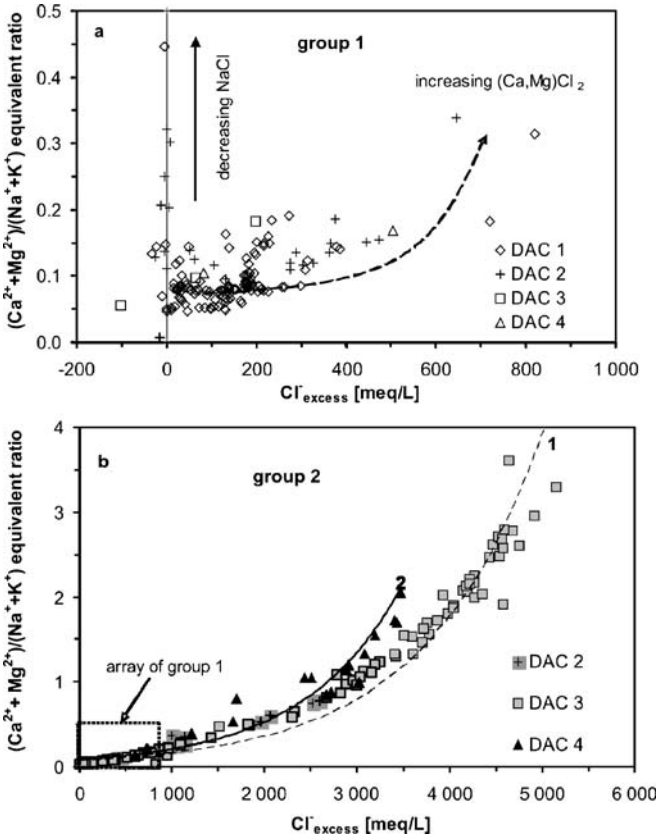

Fig. 7 Cross-plots of $(Ca^{2+}+Mg^{2+})/(Na^{+}+K^{+})$ equivalent ratio vs. Cl^{-}_{excess} in meq/L in the deep aquifer complexes (DAC 14 in Fig. 2) for samples of **a** group 1 and **b** group 2. Line *1* and line *2* indicate the observed trends. For details refer to text. Symbols are according to Fig. 3

suggest participation of these waters in processes of dolomitisation of limestone as in the following:

$$2CaCO_3 + Mg^{2+} \Leftrightarrow CaMg(CO_3)_2 + Ca^{2+} \quad (4)$$

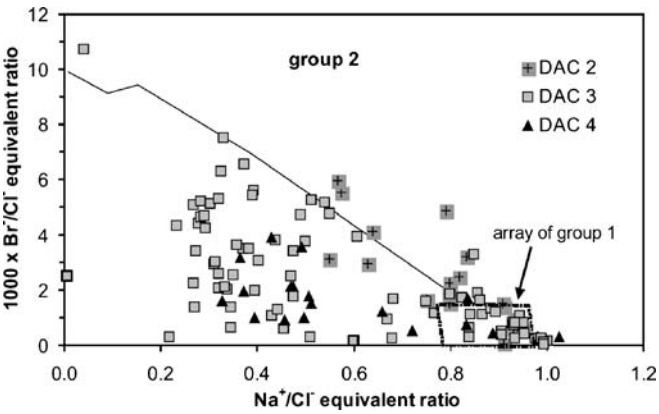

Fig. 8 Cross-plot of 1,000 × Br^{-}/Cl^{-} equivalent ratio vs. Na^{+}/Cl^{-} equivalent ratio in the deep aquifer complexes (DAC 2–4 in Fig. 2) for samples of group 2; the *box* displays the array of samples in group 1. The *line* indicates the seawater evaporation trend based on a literature compilation in Fontes and Matray (1993)

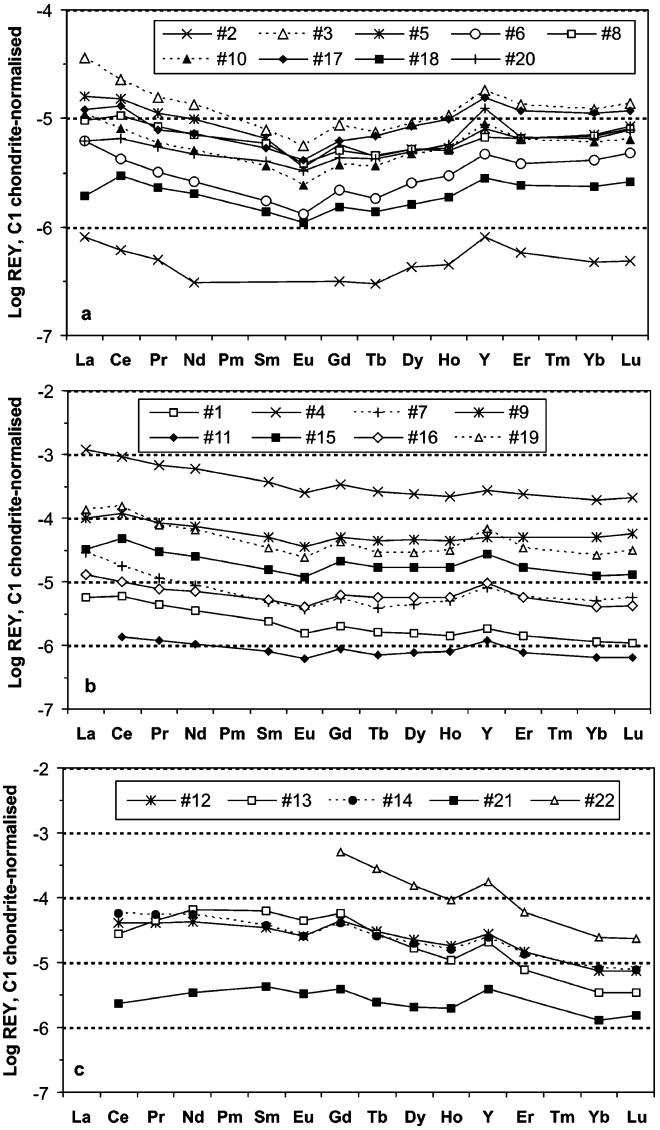

Fig. 9 Rare-earth element distribution patterns of groundwaters in Table 2. Grouping was done according to uniformity of trends: **a** type R1; **b** type R2; **c** type R3. For details, refer to text

or of albitisation of plagioclase:

$$2Na^{+} + CaAl_2SiO_8 + 4SiO_2 \Leftrightarrow 2NaAlSi_3O_8 + Ca^{2+} \quad (5)$$

Dissolution of anhydride is limited, particular in high-salinity waters, and should be paralleled by increasing sulphate contents. Figure 5a shows that Ca^{2+}/SO_4^{2-} equivalent ratios exceed unity without any systematic trends. The absence of a correlation between $Ca^{2+}$and SO_4^{2-} disproves anhydride dissolution to be important. However, bacterially mediated SO_4^{2-} reduction may obliterate any expected correlation.

The Br^{-}/Cl^{-} equivalent ratios of water samples show different arrays for both groups (Fig. 8). Any samples

 DOI 10.1007/s10040-007-0176-y

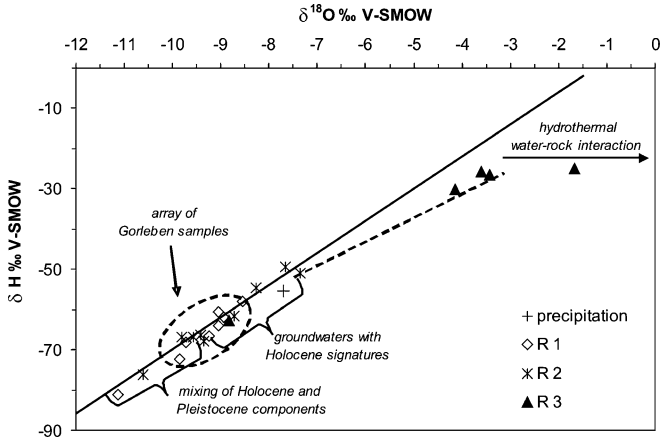

Fig. 10 Cross-plot of δ^2H vs. $\delta^{18}O$ in ‰ V-SMOW. *Solid line* represents the global meteoric water line after Craig (1961). *Dashed line* indicates a probable evaporation trend (Kyser and Kerrich 1990). Sample grouping according to the observed REY patterns (R1–R3). For comparison, the *ellipse* illustrates the array of isotope patterns found in Gorleben (Kloppmann et al. 2001)

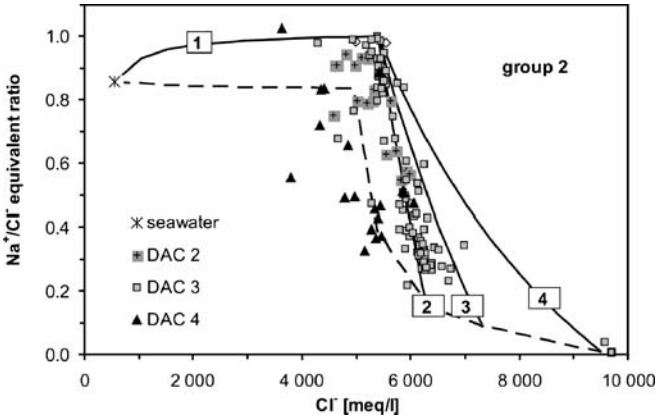

Fig. 11 Cross-plot of Na^+/Cl^- equivalent ratio vs. Cl^- in meq/L in the deep aquifer complexes (DAC 1–4 in Fig. 2) for samples of group 2. The *broken curve* displays the seawater evaporation trend. The *solid curves* represent the mixture of a saturated halite brine with (*lines*): *1* seawater, *2* a residual brine at the stage of sylvite precipitation, *3* a residual brine at the stage of carnallite precipitation, and *4* a residual brine at the stage of bischofite precipitation; based on a literature compilation in Fontes and Matray (1993)

plotting below the seawater evaporation line cannot be explained by halite dissolution. The low Na^+/Cl^- ratios indicate that besides dissolution of halite other halides are present. Like in Fig. 6, this suggests that mixing occurs with $(Ca,Mg)Cl_2$ brines which may be variable in Br^-/Cl^- ratios as shown by the two extreme Mg-rich brines with about 10,000 meq/L (Fig. 5b) with either 20 or 100 meq/L Br^- (Fig. 4e). Residual evaporation brines seem to be present only occasionally. However, the Br^-/Cl^- ratio depends on what salts are dissolved and whether Br^- is additionally gained by leaching sediments rich in organic material (e.g. Land and Prezbindowski 1981; Connolly et al. 1990; Bein and Dutton 1993). The Upper Permian brines (DAC 3) with $Mg^{2+}>>Ca^{2+}$ (Fig. 5b), and Br^-/Cl^- ratios similar to those of marine evaporation brines suggest that evaporation brines were and are still present. Additionally, one has to assume that also evaporitic salts of Mg-chlorides and -sulphate and -halite were and still are dissolved, resulting in brines with low Br^-/Cl^- ratios, much lower than those expected from evaporation brines. Judging from the wide spread of Br^-/Cl^- ratios in Fig. 8, mixtures of these two types of Mg-rich brines might have been and are still common.

The mixing relationship between different kinds of brines is separately analysed in Fig. 11 for samples of group 2. In this plot various mixing lines between the following end members are calculated by PHREQPITZ (Parkhurst and Appelo 1999): seawater and saturated halite (1), and saturated halite brine and evaporation brines at beginning of sylvite (2), carnallite (3), and bischofite (4) crystallisation (Fontes and Matray 1993). Most samples from the upper three deep aquifer complexes plot between curves 2 and 3. All DAC 4 samples (Lower Permian) plot along or left of the seawater evaporation curve. This separation widely corresponds to that in Fig. 7b.

Rare-earth elements and yttrium (REY) and stable isotopes

The REY abundance in waters is controlled by the solubility of major and accessory minerals followed by subsequent adsorption onto surfaces of rock-forming minerals and their surface coatings (Möller 2000, 2002). Any sediment is characterised by typical REY-bearing accessory minerals, and REY in water reflect the most soluble suite of such components in the recharge area. Due to their low concentrations REY easily equilibrate with mineral surfaces. Even when passing different lithologies, changes of REY in groundwater are minor, neglecting the induction period. This behaviour is similar to that of REY in an ion exchange column after the breakthrough of REY occurred. Only if large amounts of minerals are dissolved by infiltrating groundwater such as dissolution of evaporites, regional dolomitisation or albitisation, REY abundances are varied. Thus, REY distribution patterns are a useful tool in identifying the most likely group of rocks or sediments of the replenishment area (Möller et al. 2003, 2006).

Type R1 patterns (Fig. 9a) show all features of oxidative weathering of Fe(II) bearing minerals, which lead to precipitation of Fe,Mn oxyhydroxides. In this process, REY are fractionated (Bau 1999; Kawabe et al. 1999; Quinn et al. 2004). Ce(III) is oxidised to Ce(IV) and coprecipitated with FeOOH. La, Gd, Y and Lu are less coprecipitated than REE inbetween them. Furthermore, the FeOOH precipitate enriches middle REE. This results in concave patterns with negative Ce and positive Gd anomalies in the residual water. All waters of type R1 show δ^2H in the range of −64 to −76‰, which indicates mixtures of Pleistocene and Recent precipitation at depth down to about 300 m at maximum (Fig. 12).

Type R2 patterns (Fig. 9b) resemble those of the carbonates and marls (Möller et al. 2003, 2006). Stable isotopes (δ^2H: −51 to −67‰) indicate mixing of Recent

 DOI 10.1007/s10040-007-0176-y

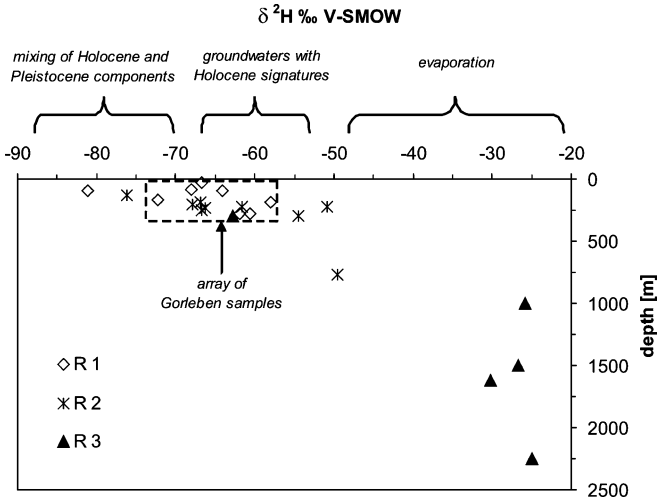

Fig. 12 Cross plot of δ^2H in ‰ VSMOW vs. depth of well in m; sample grouping according to the observed REY patterns (*R1–R3*). For comparison, the *ellipse* illustrates the array of isotope patterns found in Gorleben (Kloppmann et al. 2001)

and Pleistocene water. These mixtures are restricted to depths of about 800 m (Fig. 12).

Type R3 patterns characterise waters from Upper Triassic to Permian strata with mainly high isotope ratios (Fig. 9c) which have been sampled down to about 2,200 m (Fig. 12). In general, isotopically enriched groundwaters with respect to modern recharge are explained by warmer-than-Holocene paleorecharge temperature (Kyser and Kerrich 1990). Alternatively, Yapp and Epstein (1977) hypothesised that glacial-age meteoric waters, which precipitated over ice-free regions of North America, had more positive δ^2H values than corresponding modern waters by an average of 19‰. However, this hypothesis cannot account for the observed isotope ratios of type R3 as a thick ice shield covered the area. This leaves evaporation the only process that explains the high isotope ratios in the NEGB.

The hot brine of Neustadt-Glewe (no. 22) with δ^2H > −26.6‰ (reservoir temperature exceeds 90°C) is comparable with samples no. 12–14, whereas its δ^{18}O value (−1.72‰) is shifted by hydrothermal water–rock interaction (Taylor 1974). The sample no. 22 represents waters with the highest fraction of a deep-seated halite Ca–Cl brine or hydrothermal exchange of ^{18}O (Taylor 1974). The isotope ratios of sample no. 19 from the Upper Permian strata (Zechstein) with δ^2H=−66.6‰ and δ^{18}O=−9.8‰, indicates mixing of Pleistocene and Recent precipitation, but the REY pattern is of the R3 type. This sample originates from a depth of about 300 m. Therefore, it is most probable that Recent to Pleistocene infiltration water dissolved Zechstein salts brought to shallow depth by diapirism. Large-scale lateral flow regimes have to be assumed because all pre-Rupelian aquifer systems to a depth of at least 800 m are isotopically characterised by Recent or Pleistocene recharge conditions (Fig. 12).

Surprising is the fact that some pre-Rupelian samples such as no. 7 (Upper Triassic) and no. 20 (Lower Triassic) are strongly influenced by Pleistocene water. Bearing in mind that the Rupelian Clay is considered a low-permeability complex, it should have prohibited exchange of water between the pre- and post-Rupelian aquifer complexes, if locally eroded. Isotopic compositions of the post-Rupelian water are hydrodynamically plausible as no aquiclude separates the Quaternary and Upper Tertiary aquifers (Table 1). For example, the groundwater sample no. 8 (δ^{18}O=−9.85‰, δ^2H=−72.3‰), indicating Pleistocene precipitation conditions, belongs to a post-Rupelian Tertiary freshwater complex. However, its TDS exceeds 5 g/L, which is not explicable without assuming contribution from an underlying saline water body. Lateral saline mass transport can be excluded because all neighbouring observation wells of similar depth show freshwater. Therefore, a locally ascending flow must exist. In general, isotope distribution and REY patterns are closely linked.

Depth dependence

Excepting the groundwaters of type R3, infiltrating water has systematically replaced any formation water in the upper 800 m of sediments and sedimentary rocks. Minor fractions may still be enclosed in rocks. The infiltrating waters are salinised by mixing with local, gravity-driven ascending brines or by leaching evaporites. The REY patterns suggest that these groundwaters move between the various aquifers along hydraulic connections. Inter-aquifer flow is common in shallow aquifer systems. It can be followed down to 2,000 m as shown for group 1 samples in Fig. 3. As shown by stable isotopes and REY types, two different water bodies occur. Major elements

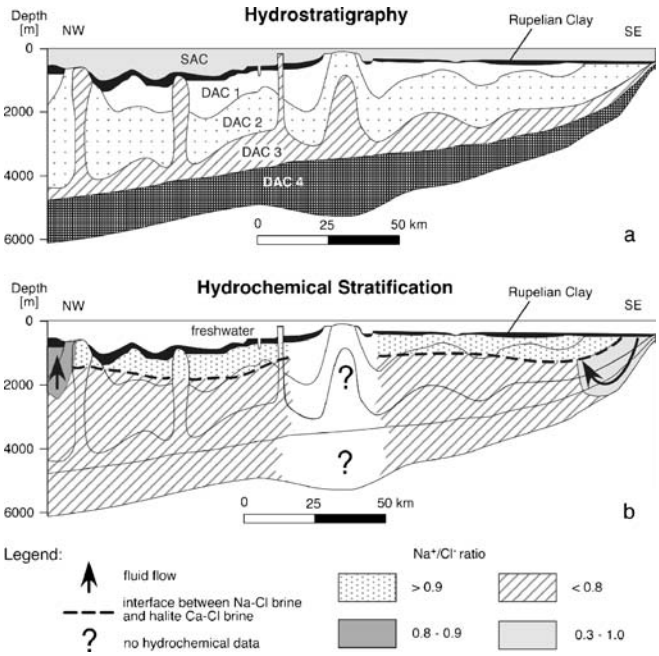

Fig. 13 Cross-section of **a** the hydrostratigraphic units (*DAC 1–4* in Fig. 2) and **b** the hydrochemical stratification in the study area. The cross-section runs from the margin of the NEGB in the *SE* towards the centre in the *NW* (as indicated in Fig. 1); modified after Manhenke (2002)

DOI 10.1007/s10040-007-0176-y

clearly separate brines into two groups, which are distinctly different in Na^+/Cl^- equivalent ratios. Group 1 ($Na^+/Cl^->0.9$) and group 2 ($Na^+/Cl^-<0.8$) represent a halite and halite Ca–Cl type of water, respectively. Thus, three different criteria prove the presence of two different water bodies with an interface varying between 800 and 1,500 m (Fig. 13).

The interface is nearly independent of geologic formations (Fig. 13a and b). The gravity-flow system is sustained by meteoric recharge at the SE of the study area. Consequently, the Upper Permian deposits (DAC 3) at higher elevations near the margin of the basin have undergone dissolution by the circulating meteoric waters. This has resulted in disturbed overlying strata, chaotic bedding, faults and numerous joints (Voigt 1975). Some waters leaks into the Lower Permian strata (DAC 4). It is assumed that upward directed brine movement along with mixing processes are responsible for the large scatter in Na^+/Cl^- equivalent ratios at the SE margin of the basin (Fig. 13b). In the NW, intermediate Na^+/Cl^- equivalent ratios are encountered close to a salt diapir at shallow depth. Brines with intermediate Na^+/Cl^- equivalent ratios of ~0.84–0.88 might be either gypsum Ca–Cl brine or a mixture of Na–Cl brine and halite Ca–Cl brine (Bein and Dutton 1993). The data analysis does not support the existence of gypsum Ca–Cl brine. Therefore, mixing between Na–Cl brines and halite Ca–Cl brines seems reasonable. It is suggested that local faults, commonly flanking salt diapirs, serve as groundwater conduits. Thermally driven convection near salt domes in the NEGB presents a simple and plausible transport mechanism, provided salinity effects do not overhelm the thermal effects (Magri et al. 2005a,b).

If the stratigraphy is reduced to Rupelian as the main aquiclude of the near-surface systems, it turns out that:

- Groundwater samples from post-Rupelian aquifers largely represent mixtures of Recent and Pleistocene precipitation, and
- Groundwater samples from pre-Rupelian aquifers cover the whole range of isotope data shown in Fig. 12. The samples represent water from different geologic times and mixtures of these waters with Pleistocene precipitation, and have experienced isotopic changes locally, e.g. by evaporation prior to infiltration or by hydrothermal overprinting.

Conclusions

Halite and halite Ca–Cl brines cause salinisation of groundwater in the NE German Basin.

The salinity of halite brines increases with depth from Cretaceous to Upper Triassic (Keuper) but is not restricted to stratigraphic units. Only the salinity of waters from Upper Permian strata is independent of depth, although some of the samples are from depths of <1,000 m. Waters from the Lower Triassic represent a link between the two groups.

The halite brines originate from dissolution of Permian evaporites with very low Br^-/Cl^- ratios by percolating water. Some mixing with evolved evaporation brine may also occur. Thus, formation brines are still present but are not dominant.

The Ca–Cl brines show high hydrochemical diversity. Locally, the $MgCl_2$ brines with high Br^-/Cl^- ratios represent evaporation brines in a strict sense. The Ca–Cl brines evolved from evaporation brines by chemical interaction with the aquifer environment and dolomitisation of limestones is the most common process.

Conjointly, interpretation of stable H and O isotopes ratios and REY patterns suggest that many groundwaters in Quaternary to Lower Triassic units evolved from infiltrating meteoric waters. The post-Rupelian groundwater largely represents mixtures of Recent and Pleistocene precipitation. The Rupelian is considered the main aquiclude of the near-surface systems, which separates fresh and saline groundwater bodies. The pre-Rupelian waters, however, cover the whole range of isotope data and REY distribution patterns. The presence of isotope patterns typical for Pleistocene to Recent replenishment in the pre-Rupelian aquifers indicates infiltration of surface water in places where the Rupelian Clay is absent and large-scale groundwater flow regimes may exist. All saline waters studied in detail indicate that they are younger than the formations in which they occur.

Interaquifer flow is proved by stable H and O isotopes and by REY patterns, especially in the shallow aquifers. However, even at depths exceeding 2,000 m, interaquifer flow is recognisable. In general, interpolation of REY patterns coincides well with those of isotope ratios.

Acknowledgements The German Science Foundation (DFG) supported this project as part of the SPP 1135 "Dynamics of Sedimentary Systems under Varying Stress Conditions by Example of the Central European Basin System". We also acknowledge the help of the Geological Surveys of Berlin (SenStadt Berlin), Brandenburg (LGRB) and Saxony Anhalt (LAGB). We would like to thank the well maintenance companies of Bad Saarow, Bad Wilsnack, Belzig, Templin and Waren for access to their facilities. We gratefully acknowledge the critical comments of three anonymous reviewers.

References

Anders E, Grevesse N (1989) Abundance of elements: meteoric and solar. Geochim Cosmochim Acta 53:197–214

Bassett RL, Bentley ME (1982) Geochemistry and hydrodynamics of deep formation brines in the Palo Duro Basin and Dalhart Basins, Texas, USA. J Hydrol 59:331–372

Bau M (1999) Scavenging of dissolved yttrium and rare earths by precipitating iron oxyhydroxides: experimental evidence for Ce oxidation, Y-Ho fractionation, and lanthanide tetrad effect. Geochim Cosmochim Acta 63:67–77

Bau M, Dulski P (1996) Anthropogenic origin of positive gadolinium anomalies in river waters. Earth Planet Sci Lett 143:245–255

Beer H, Manhenke V (2001) Erdwärme-und Thermalsolnutzung in Ostbrandenburg [Geothermal and hydrothermal resources in East Brandenburg]. Zt Geol Wiss 29:211–222

Bein A, Dutton AR (1993) Origin, distribution, and movement of brine in the Permian Basin (U.S.A.): a model for displacement of connate brine. Geol Soc Amer Bull 105:695–707

Bennett SS, Hanor JS (1987) Dynamics of subsurface salt dissolution at the Welsh Dome, Lousiana Gulf Coast. In: Lerch I, O'Brien JJ (eds) Dynamical geology of salt and related structures, Academic Press, Orlando, FL, USA, pp 653–677

Bourg C, Stievenard M, Jouzel J (2001) Hydrogen and oxygen isotopic composition of aqueous salt solutions by gas-water equilibration method. Chem Geol 173:331–337

Carpenter AB (1978) Origin and chemical evolution of brines in sedimentary basins. Oklahoma Geol Surv Bull 79:60–77

Clayton RN, Friedmann I, Graf DL, Mayeda TK, Meents WF, Shimp NF (1966) The origin of saline formation waters. J Geophys Res 71:3869–3882

Connolly CA, Walter LM, Baadsgaard H, Longstaffe FJ (1990) Origin and evolution of formation waters, Alberta Basin, Western Canada Sedimentary Basin. I. Chemistry. Appl Geochem 5:397–413

Craig H (1961) Isotopic variations in meteoric waters. Science 133:1702–1703

Domenico PA, Robbins GA (1985) The displacement of connate water from aquifers. Geol Soc Amer Bull 96:328–335

Dulski P (1994) Interferences of oxide, hydroxide and chloride analyte species in the determination of rare earth elements in geological samples by inductively coupled plasmamass spectrometry. Fresenius' J Anal Chem 350:194–203

Dulski P (2001) Reference materials for Geochemical studies: new analytical data by ICP-MS and critical discussion of reference values. Geostand Newsl 25:87–125

Evans D, Nunn J (1989) Free thermohaline convection in sediments surrounding a salt column. J Geophys Res 94:12413–12422

Fontes JC, Matray JM (1993) Geochemistry and origin of formation brines from the Paris basin, France, 1: brines associated with Triassic salts. Chem Geol 109:149–175

Glander H, Schirrmeister W (1975) Erfassung und Darstellung der oberen Mineralwassergrenzfläche [Delineation and mapping of the upper fresh-/saltwater interface]. Zt Angew Geol 21:322–334

Graf DL, Meents WF, Friedman I, Shimp NF (1966) The origin of saline formation waters III: calcium-chloride waters. US Geol Surv Circ 397:60

Grube A, Lotz B (2004) Geological and numerical modeling of geogenic salinisation in the area of the Lübeck basin (North Germany). Groundwater and saline intrusion. Selected papers from the 18th Salt Water Intrusion Meeting (SWIM), Cartagena, Spain, 31 May–3 June 2004, pp 183–195

Grube A, Wichmann K, Hahn J, Nachtigall KH (2000) Geogene Grundwasserversalzung in den Porengrundwassserleitern Norddeutschlands und ihre Bedeutung für die Wasserwirtschaft [Geogenic groundwater salinisation of porous aquifer systems and its impact on water management]. Technologiezentrum Wasser Karlsruhe (TZW), Karlsruhe, Germany, 203 pp

Hannemann M, Schirrmeister W (1998) Paläohydrogeologische Grundlagen der Entwicklung der Süß-/Salzwassergrenze und der Salzwasseraustritte in Brandenburg [Paleo-hydrogeological principles of the development of the fresh-/saltwater interface and the occurrence of saline springs in Brandenburg]. Brandenbg Geowiss Beitr 5:61–72

Hanor JS (1994a) Origin of saline fluids in sedimentary basins. In: Parnell J (ed) Geofluids: origin, migration and evolution of fluids in sedimentary basins. Geol Soc Spec Publ 78:151–178

Hanor JS (1994b) Physical and chemical controls on the composition of waters in sedimentary basins. Mar Pet Geol 11:31–46

Hennebrüder K, Wennrich R, Mattusch J, Stärk HJ, Engewald W (2004) Determination of gadolinium in river water by SPE preconcentration and ICP-MS. Talanta 63:309–316

Hoth P, Seibt A, Kellner T, Huenges E (1997) Geothermie Report 97-1: Geowissenschaftliche Bewertungsgrundlagen zur Nutzung hydrogeothermaler Resourcen in Norddeutschland [Basis of geoscientific evaluation for using geothermal resources in northern Germany]. Sci Tech Rep 15:1–149

Kaiser R (2001) Fazies und Sequenzstratigraphie: Das Staßfurtkarbonat (Ca2) am nördlichen Beckenrand des südlichen Zechsteinbeckens (NE-Deutschland) (Facies and sequence stratigraphy: the Staßfurtcarbonate (Ca2) at the northern margin of the southern evaporite basin of Upper Permian). PhD Thesis, Universität Köln, Germany

Kawabe I, Ohta A, Miura N (1999) Distribution coefficients of REE between Fe oxyhydroxide precipitates and NaCl solutions affected by REE-carbonate complexation. Geochem J 33:181–197

Kharaka YK, Berry FAF (1973) Simultaneous flow of water and solutes through geological membranes: I. experimental investigations. Geochim Cosmochim Acta 37:2577–2603

Klinge H, Vogel P, Schelkes K (1992) Chemical composition and origin of saline formation waters from the Konrad mine, Germany. Water–Rock Interaction, Proceedings of the 7th International Symposium on Water–Rock Interaction/WRI-7, Park City, Utah, USA, 13–18 July 1992, pp 1117–1120

Klinge H, Schelkes K, Rübel A, Suckow A, Schildknecht F, Ludwig R (2002) The saltwater/freshwater regime in the sedimentary cover of the Gorleben Salt Dome. Transp Porous Media 47:125–148

Kloppmann W, Negrel P, Casanova J, Klinge H, Schelkes K, Guerrot C (2001) Halite dissolution derived brines in the vicinity of a Permian salt dome (N German Basin): evidence from boron, strontium, oxygen, and hydrogen isotopes. Geochim Cosmochim Acta 65:4087–4101

Knauth LP (1988) Origin and mixing history of brines, Palo Duro Basin, Texas, USA. Appl Geochem 3:455–474

Kühn M (1997) Geochemische Folgereaktionen bei der hydrothermalen Energiegewinnung [Successive geochemical reactions during utilization of hydrogeothermal energy]. Berichte aus dem Fachbereich Geowissenschaften Universität Bremen, Bremen, Germany, pp 1–129

Kyser T, Kerrich R (1990) Geochemistry fluids in tectonically active crustal regions. In: Nesbitt B (ed) Short course in fluids in tectonically active regimes of the continental crust, vol 18, AMC, Quebec, pp 133–230

Land LS (1987) The major ion chemistry of saline brines in sedimentary basins. In: Proc. Amer. Inst. of Physics, Conf., Physics and chemistry of porous media II, Schlumberger-Doll, Ridgefield, CT, USA, pp 160–179

Land LS (1992) Saline formation waters in sedimentary basins: connate or diagenetic. Water Rock Interaction-Proceedings of the 7th International Symposium on Water–Rock Interaction/WRI-7, Park City, UT, USA, 13–18 July 1992, pp 865–868

Land LS, Macpherson GL (1992) Origin of saline formation waters, Cenozoic section, Gulf of Mexico sedimentary basin. Am Assoc Pet Geol Bull 76:1344–1362

Land LS, Prezbindowski DR (1981) The origin and evolution of saline formation water, Lower Cretaceous carbonates, south-central Texas, USA. J Hydrol 54:51–74

Lehmann H-W (1974a) Geochemie und Genese der Tiefenwässer der Nordostdeutschen Senke-Teil 1 [Geochemistry and genesis of deep seated brines in the North-East German Basin, part 1]. Zt Angew Geol 20:502–509

Lehmann H-W (1974b) Geochemie und Genesis der Tiefenwässer der Nordostdeutschen Senke-Teil 2 [Geochemistry and genesis of deep seated brines in the North-East German Basin, part 2]. Zt Angew Geol 20:551–557

Löhnert E, Bauhus W, Sonntag C (1986) Mechanism of groundwater salinisation in the Hamburg region, F.R. Germany: facies and new findings. Proc of the 9th Salt Water Intrusion Meeting (SWIM), Delft Univ. of Technology, The Netherlands, pp 613–628

Magri F, Bayer U, Clausnitzer C, Jahnke C, Diersch HJ, Fuhrmann J, Möller P, Pekdeger A, Tesmer M, Voigt HJ (2005a) Deep reaching fluid flow close to convective instability in the NE German Basin: results from water chemistry and numerical modelling. Tectonophysics 397:5–20

Magri F, Bayer U, Jahnke C, Clausnitzer V, Diersch HJ, Fuhrman J, Möller P, Pekdeger A, Tesmer M, Voigt HJ (2005b) Fluid-dynamics driving saline water in the North East German Basin. Int J Earth Sci 94:1056–1069

Manhenke V (2002) Geologie und Geopotenziale in Brandenburg-Das Geopotenzial Brandenburgs [Geology and geopotential in Brandenburg-Brandenburg's geopotential]. In: Stackebrandt W, Manhenke V (eds) Atlas zur Geologie von Brandenburg, vol 2.

Landesamt für Geowissenschaften und Rohstoffe Brandenburg, Kleinmachnow, Germany, pp 72–73
Mehta S, Fryar AE, Banner JL (2000) Controls on the regional-scale salinisation of the Ogallala aquifer, Southern High Plains, Texas, USA. Appl Geochem 15:849–864
Meyer H, Schönicke L, Wand U, Hubberten H, Friedrichsen H (2000) Isotope studies of hydrogen and oxygen in ground ice: experiences with the equilibration technique. Isot Environ Health Stud 36:133–149
Möller P (2000) Rare earth elements and yttrium as geochemical indicators of the souce of mineral and thermal waters. In: Stober I, Bucher K (eds) Hydrology of crystalline rocks, Kluwer, Dordrecht, pp 227–246
Möller P (2002) The distribution of rare earth elements and yttrium in water-rock interactions: field observations and experiments. In: Stober I, Bucher K (eds) Water-rock interaction, Kluwer, Dordrecht, pp 97–123
Möller P, Dulski P, Morteani G (2003) Partitioning of rare earth elements yttrium and some major elements among source rocks, liquid and vapor of Lardello-Travale Geothermal Field, Tuscany (central Italy). Geochim Cosmochim Acta 67:171–183
Möller P, Woith H, Dulski P, Lüders V, Erzinger J, Kämpf H, Pekdeger A, Hansen B, Lodemann M, Banks D (2005) Main and trace elements in KTB-VB fluid: composition and hints to its origin. Geofluids 5:28–41
Möller P, Dulski P, Salameh E, Geyer S (2006) Characterization of thermal spring- and well water in Jordan by rare earth element and yttrium distribution and stable isotopes of H2O. Acta Hydrochim Hydrobiol 34:101–116
Neumann E (1975) Hydrogeologische Verhältnisse des Paläozoikums und Mesozoikums am Nordrand der Norddeutsch-Polnischen Senke und ihre Beziehungen zu den Erdöl- und Erdgasvorkommen [Hydrogeological settings of the Palaeozoic and Mesozoic strata in respect to the oil and gas resources at the northern boundary of the German-Polish basin]. PhD Thesis, Bergakademie Freiberg, Germany
Naumann D (2000) Salinare Tiefenwässer in Norddeutschland: gas- und isotopengeochemische Untersuchungen zur Herkunft und geothermischen Nutzung [Deep seated brines in northern Germany: gas and isotopes studies to evaluate genesis and geothermal potential]. Sci Tech Rep 00/21, GeoForschungsZentrum Potsdam, Potsdam, Germany, pp 1–116
Nishri A, Herbert HJ, Jockwer N, Stichler W (1988) The geochemistry of brines and minerals from the Asse Salt Mine, Germany. Appl Geochem 3:317–332
Parkhurst DL, Appelo CAJ (1999) User's guide to PHREEQC (Verion 2): a computer program for speciation, batch-reaction, one dimensional transport and inverse geochemical calculations. USGS Water-Resources Invest Rep 99–4259, 312 pp
Quinn KA, Byrne RH, Schijf J (2004) Comparative scavenging of yttrium and the rare earth elements in seawater: competitive influences of solution and surface chemistry. Aquatic Chem 100:59–80
Rieke H, Kossow D, McCann T, Krawczyk C (2001) Tectono-sedimentary evolution of the northernmost margin of the NE German Basin between uppermost Carboniferous and Late Permian (Rotliegend). Geol J 36:19–38
Rizkalla EN, Choppin GR (1991) Hydration and hydrolyse of lanthanides. In: Gschneidner KA, Eyring LJ, Hüfner S (eds) Handbook of physics and chemistry of rare earths, North-Holland, Amsterdam, 15:391–442
Scheck M, Bayer U (1999) Evolution of the Northeast German Basin: inferences from a 3D structural model and subsidence analysis. Tectonophysics 313:145–168
Scheck M, Barrio-Alvers L, Bayer U, Götze HJ (1999) Density structure of the Northeast German Basin: 3D modelling along the DEKORP line BASIN96. Phys Chem Earth Part A 24:221–230
Schmidt Mumm A, Wolfgramm M (2002) Diagenesis and fluid mobilisation during the evolution of the North German Basin: evidence from fluid inclusion and and sulphur isotope analysis. Mar Petrol Geol 19:229–246
Senger RK (1991) Regional hydrodynamics of variable-density flow systems, Palo Duro Basin, Texas. The University of Texas at Austin Bureau of Economic Geology Report of Investigation, vol 202. University of Texas, Austin, TX, USA, 54 pp
Shabani MB, Agaki T, Shimuzu H, Masuda A (1990) Determination of trace lanthanides and yttrium in seawater by inductively coupled plasma mass spectrometry after preconcentration with solvent extraction and back-extraction. Anal Chem 62:2709–2714
Spencer RJ (1987) Origin of Ca–Cl brines in Devonian formations, western Canada sedimentary basin. Appl Geochem 2:373–384
Stackebrandt W, Lippstreu L (2002) Geologie und Geopotenziale in Brandenburg-Zur geologischen Entwicklung Brandenburgs [Geology and geopotentials in Brandenburg-Brandenburg's geopotentials-Brandenbrug's gelogic evolution]. In: Stackebrandt W, Manhenke V (eds) Atlas zur Geologie von Brandenburg, vol 2. Landesamt für Geowissenschaften und Rohstoffe Brandenburg, Kleinmachnow, Germany, pp 19–24
Stueber AM, Walter LM, Huston TJ, Pushkar P (1993) Formation waters from Mississipian-Pennsylvanian reservoirs, Illinois basin, USA: chemical and isotopic constraints on evolution and migration. Geochim Cosmochim Acta 57:763–784
Taylor HP (1974) The application of oxygen and hydrogen isotope studies to problems of hydrothermal alteration and ore deposits. Econ Geol 69:843–883
Toth J (1980) Cross-formational gravity flow of ground water: a mechanism of the transport and accumulation of petroleum (the generalized hydraulic theory of petroleum migration). In: Roberts WH III, Cordell RJ (eds) Problems of petroleum migration. AAPG studies in Geology no. 10, AAPG, Tulsa, OK, USA, pp 121–167
Trettin R, Hill A, Wolf M, Deibel K, Glässer W (1997) Isotopenanalytische Charakterisierung tiefliegender Grundwässer im Raum der Fürstenwalde-Gubener Störungszone [Isotopical characterisation of deeper groundwater in the area of the Fürstenwalde-Gubener fault zone]. Zt Grundwasser 2:65–76
Voigt HJ (1972) Genese und Hydrochemie mineralisierter Grundwässer [Genesis and hydrochemistry of saline groundwater]. Zentrales Geologisches Institut Berlin, Berlin, pp 1–150
Voigt HJ (1975) Zur Dynamik mineralisierter Schichtenwässer im Nordteil der DDR [Dynamics of saline formation water]. Zt Angew Geol 21:164–167
Voigt HJ (1977) Zur Geochemie der Spurenelemente Brom, Iod, Strontium und Lithium in den Mineralwässern des Nordteils der DDR [Geochemistry of the trace elements bromine, iodine, boron, strontium and lithium in brines of the northern part of the German Democratic Republic]. Zt Angew Geol 23:395–402
Vosteen H-D, Rath V, Schmidt Mumm A, Clauser C (2004) The thermal regime of the Northeastern-German Basin from 2-D inversion. Tectonophysics 386:81–95
Warren EA, Smalley PC (1992) Spatial variations in north Sea formation water composition. Water Rock Interaction, Proceedings of the 7th International Symposium on Water–Rock Interaction/ WRI-7, Park City, UT, USA, 13–18 July 1992, pp 1129–1132
Wilson TP, Long DT (1992) Geochemistry and isotope chemistry of Michigian Basin brines: Devonian formations. Appl Geochem 7:81–100
Yapp CJ, Epstein S (1977) Climatic implications of D/H ratios of meteoric water over North America (9500-22,000 B.P.) as inferred from ancient wood cellulose C-H hydrogen. Earth Planet Sci Lett 34:333–350
Zieschang J (1974) Ergebnisse und Tendenzen hydrogeologischer Forschungen in der DDR [Results and tendencies of hydrogeological research in the GDR]. Zt Angew Geol 20:452–458